ELSEVIER

Engineering Analysis with Boundary Elements 28 (2004) 1335–1350

ENGINEERING ANALYSIS *with* BOUNDARY ELEMENTS

www.elsevier.com/locate/enganabound

Symmetric Galerkin boundary element computation of T-stress and stress intensity factors for mixed-mode cracks by the interaction integral method

Alok Sutradhar, Glaucio H. Paulino*

Newmark Civil Engineering Laboratory, Department of Civil and Environmental Engineering, University of Illinois at Urbana-Champaign, MC-250, 205 North Mathews Avenue, Urbana, IL 61801-2352, USA

Received 10 November 2003; revised 17 February 2004; accepted 23 February 2004

Available online 11 June 2004

Abstract

An interaction integral method for evaluating T-stress and mixed-mode stress intensity factors (SIFs) for two-dimensional crack problems using the symmetric Galerkin boundary element method is presented. By introducing a known auxiliary field solution, the SIFs for both mode I and mode II are obtained from a path-independent interaction integral entirely based on the $J(\equiv J_1)$ integral. The T-stress can be calculated directly from the interaction integral by simply changing the auxiliary field. The numerical implementation of the interaction integral method is relatively simple compared to other approaches and the method yields accurate results. A number of numerical examples with available analytical and numerical solutions are examined to demonstrate the accuracy and efficiency of the method.
© 2004 Elsevier Ltd. All rights reserved.

Keywords: Fracture mechanics; Mixed-mode stress intensity factors; T-stress; Symmetric Galerkin boundary element method; Interaction integral (M-integral); Two-state integral

1. Introduction

Fracture behaviour is generally characterized by a single parameter such as the stress intensity factors (SIFs) or path-independent J-integral [1]. These quantities provide a measure of the dominant behaviour of the stress field in the vicinity of a crack-tip. In order to understand the effect of the structural and loading configuration on the 'constraint' [2] conditions at the crack-tip, another parameter is required. A second fracture parameter often used is the elastic T-stress. In two dimensions, the T-stress is defined as a constant stress acting parallel to the crack and its magnitude is proportional to the nominal stress in the vicinity of the crack. Various studies have shown that the T-stress has significant influence on crack growth direction, crack growth stability, crack-tip constraint and fracture toughness [3–8]. In order to calculate the T-stress, researchers have used several techniques such as the stress substitution method [9], the variational method [10], the Eshelby J-integral method [11,12], the weight function method [13], the line spring method [14], the Betti–Rayleigh reciprocal theorem [15,16], and the interaction integral method [15,17]. Among these methods, the Eshelby J-integral method, the Betti–Rayleigh reciprocal theorem and the interaction integral method are based on path-independent integrals. In these methods, the fracture parameters can be calculated using data remote from the crack-tip and, as a result, higher accuracy compared to local methods can be achieved.

For a few idealized cases, analytical solutions for T-stress and SIFs are available. However, for practical problems involving finite geometries with complex loading, numerical methods need to be employed. The boundary element method (BEM) has emerged as a powerful numerical method for computational fracture analysis. In BEM analysis, only the boundary of the domain is discretized and unknown quantities are determined only on the boundaries. Compared to domain-type methods (e.g. finite element method (FEM) and meshless methods [18]), this boundary method significantly reduces the problem size and the problem setup. Additionally, remeshing of propagating cracks, which only involves local operations on

* Corresponding author. Tel.: +1-217-333-3817; fax: +1-217-265-8041.
E-mail address: paulino@uiuc.edu (G.H. Paulino).

0955-7997/$ - see front matter © 2004 Elsevier Ltd. All rights reserved.
doi:10.1016/j.enganabound.2004.02.009

the propagating tip/front region, is simple and easy. The Galerkin BEM has several advantages over the collocation BEM. The biggest advantage is that the hypersingular integrals can be evaluated using standard C^0 elements without any compromise or ambiguity [19]. Moreover, the weighted averaging formula in the Galerkin BEM provides a reliable solution in the neighborhood of geometric discontinuities such as corners and junctions. The Galerkin approach involves one more integration compared to collocation. The symmetric Galerkin BEM (SGBEM) uses both the standard singular displacement boundary integral equation (BIE) and the hypersingular traction BIE in such a way that the resultant coefficient matrix for the linear system becomes symmetric. The symmetry property of the coefficient matrix reduces the computation time of the problem. Also by exploiting symmetry [20] and using faster algorithms [21] in setting up the coefficient matrix, computational effort can be further reduced. This paper is based on the SGBEM [22–25], and follows the approach of Ref. [26]. A recent review [19] provides an excellent introduction to the literature on the SGBEM.

The interaction integral method is based on conservation laws of elasticity and fundamental relationships in fracture mechanics [27]. SIFs pertaining to mixed-mode fracture problems can be easily obtained from this integral. The basis of the approach lies in the construction of a conservation integral for two superimposed states (actual and auxiliary) of a cracked elastic solid. The analysis requires integration along a suitably selected path surrounding the crack-tip. The method was originally proposed by Chen and Shield [27], and later implemented numerically by Yau et al. [28] using the FEM applied to homogenous isotropic materials. Since then, this method has been used by many other researchers. For instance, Wang et al. [29] applied the method to anisotropic materials, and Gosz and Moran [30] investigated three-dimensional (3D) interface cracks. Recently this method has been widely used to determine mixed-mode SIFs in functionally graded materials (FGMs). Dolbow and Gosz [31] originally developed it with the extended FEM (X-FEM). Rao and Rahman [32] implemented this method using the element free Galerkin (EFG) method. Kim and Paulino [33,34] used the method to solve mixed-mode crack problems in isotropic and orthotopic FGMs in conjunction with the FEM and micromechanics models. They have also extended the two-state integral approach to evaluate T-stress in isotropic [35,36] and orthotopic [37] FGMs.

In the BEM literature, the displacement correlation technique (DCT) is widely used to evaluate SIFs due to its simplicity in numerical implementation [38]. Among the path-independent integral techniques, Aliabadi [39] applied the J-integral to mixed-mode crack problems by decoupling the J into its symmetrical and anti-symmetrical portions. Sladek and Sladek [40] used the conservation integral method in thermoelasticity problems to calculate the T-stress, and the J-integral to calculate the SIFs. Denda [41] implemented the interaction integral for mixed-mode analysis of multiple cracks in anisotropic solids using a dislocation and point force approach (Lekhnitskii–Eshelby–Stroh formalism). Wen and Aliabadi [42] proposed a different contour integral based on Westergaard's solution and Betti's reciprocal theorem to calculate the SIFs. Reviews of the application of the BEM in fracture can be found in Refs. [43,44]. In this paper, we develop a unified scheme by using the interaction integral method for calculating both the T-stress and the SIFs for mixed-mode cracks by means of the SGBEM. Recently, Gray et al. [26] proposed a modified quarter-point element for a more accurate representation of the crack opening displacement. The present methodology also includes this improved crack-tip element.

The remaining sections of this paper are organized as follows. Section 2 provides the definition of the T-stress. The interaction integral (called M-integral) method for calculating the fracture parameters is described in Section 3. Section 4 gives an introduction to the SGBEM, followed by the SG formulation for fracture and selected features of the modified quarter-point element. Section 5 presents various numerical examples in which the T-stress and the SIFs are evaluated by means of the M-integral. Finally, Section 6 concludes with some closing remarks and potential extensions. The Appendices A–D supplement the paper.

2. Fracture parameters: T-stress and stress intensity factors

Williams' asymptotic solution [45] for crack-tip stress fields in any linear elastic body is given by a series of the form

$$\sigma_{ij}(r,\theta) = A_1 r^{-1/2} f_{ij}^{(1)}(\theta) + A_2 f_{ij}^{(2)}(\theta) + A_3 r^{1/2} f_{ij}^{(3)}(\theta) + \text{higher order terms}, \tag{1}$$

where σ_{ij} is the stress tensor, r and θ are polar coordinates with the origin at the crack-tip as shown in Fig. 1, $f_{ij}^{(1)}, f_{ij}^{(2)}, f_{ij}^{(3)}$ are universal functions of θ, and A_1, A_2, A_3 are parameters proportional to the remotely applied loads. In the vicinity of the crack ($r \to 0$), the leading term which exhibits a square-root singularity dominates. The amplitude of the singular stress fields is characterized by the stress intensity factors (SIFs), i.e.

$$\sigma_{ij} = \frac{K_{\mathrm{I}}}{\sqrt{2\pi r}} f_{ij}^{\mathrm{I}}(\theta) + \frac{K_{\mathrm{II}}}{\sqrt{2\pi r}} f_{ij}^{\mathrm{II}}(\theta), \tag{2}$$

where K_{I} and K_{II} are the mode I and mode II SIFs, respectively.

The second term in the Williams' series solution (Eq. (1)) is a non-singular term, which is defined as the elastic T-stress. Thus, the above expression (2) can be expanded to

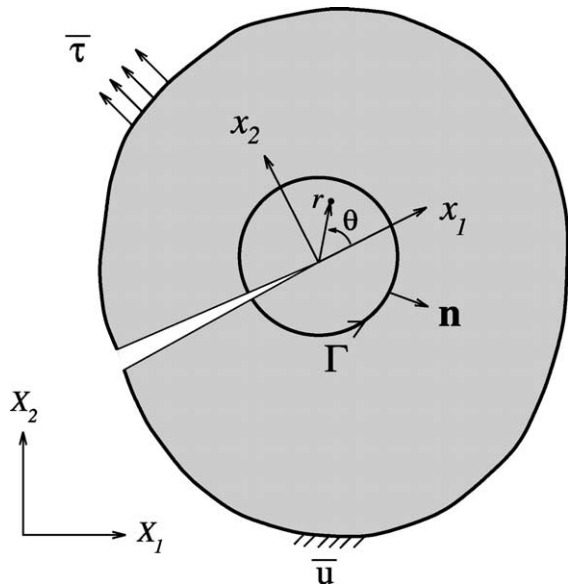

Fig. 1. Schematic of integration path and coordinate systems. Notice the Cartesian (x_1, x_2) and polar (r, θ) coordinate systems at the crack-tip. The notation $\bar{u}$ denotes prescribed displacements and $\bar{\tau}$ denotes prescribed tractions.

include this term as follows:

$$\sigma_{ij} = \frac{K_{\mathrm{I}}}{\sqrt{2\pi r}} f_{ij}^{\mathrm{I}}(\theta) + \frac{K_{\mathrm{II}}}{\sqrt{2\pi r}} f_{ij}^{\mathrm{II}}(\theta) + T\delta_{1i}\delta_{1j}. \tag{3}$$

The T-stress varies with different crack geometries and loadings. It plays a dominant role on the shape and size of the plastic zone, the degree of local crack-tip yielding, and also in quantifying fracture toughness. For mixed-mode problems, the T-stress contributes to the tangential stress and, as a result, it affects the crack growth criteria. By normalizing the T-stress with the applied load $\sigma_0 (= K_{\mathrm{I}}/\sqrt{\pi a})$, a non-dimensional parameter B can be defined by [2,10]

$$B = T\sqrt{\pi a}/K_{\mathrm{I}}, \tag{4}$$

where a is the crack length. The dependence on geometrical configurations can be best indicated by the biaxiality parameter B.

3. The two-state interaction integral: M-integral

The interaction integral or M-integral is derived from the path-independent J-integral [1] for two admissible states of a cracked elastic FGM body. The formulation of the M-integral is presented here followed by techniques to calculate T-stress and SIFs. Finally, some aspects of the numerical scheme adopted for the implementation of the contour integral are discussed.

3.1. Basic formulation

The path-independent J-integral [1] is defined as

$$J = \lim_{\Gamma \to 0} \int_{\Gamma} (\mathscr{W}\delta_{1j} - \sigma_{ij} u_{i,1}) n_j \, \mathrm{d}\Gamma, \tag{5}$$

where $\mathscr{W}$ is the strain energy density given by

$$\mathscr{W} = \int_0^{\varepsilon_{kl}} \sigma_{ij} \, \mathrm{d}\varepsilon_{ij} \tag{6}$$

and n_j denotes the outward normal vector to the contour Γ, as shown in Fig. 1.

If two independent admissible fields are considered where the displacements, strains and stresses of the actual fields and the auxiliary fields are denoted by $(\mathbf{u}, \boldsymbol{\varepsilon}, \boldsymbol{\sigma})$ and $(\mathbf{u}^{\mathrm{aux}}, \boldsymbol{\varepsilon}^{\mathrm{aux}}, \boldsymbol{\sigma}^{\mathrm{aux}})$, respectively, then the J-integral of the superimposed fields (actual and auxiliary) can be written as:

$$J^{\mathrm{s}} = \int_{\Gamma} \left\{ \frac{1}{2}(\sigma_{ik} + \sigma_{ik}^{\mathrm{aux}})(\varepsilon_{ik} + \varepsilon_{ik}^{\mathrm{aux}})\delta_{1j} - (\sigma_{ij} + \sigma_{ij}^{\mathrm{aux}}) \times (u_{i,1} + u_{i,1}^{\mathrm{aux}}) \right\} n_j \, \mathrm{d}\Gamma. \tag{7}$$

This integral can be conveniently decomposed into

$$J^{\mathrm{s}} = J + J^{\mathrm{aux}} + M, \tag{8}$$

where J is given by Eq. (5), J^{aux} is given by

$$J^{\mathrm{aux}} = \int_{\Gamma} (\mathscr{W}^{\mathrm{aux}}\delta_{1j} - \sigma_{ij}^{\mathrm{aux}} u_{i,1}^{\mathrm{aux}}) n_j \, \mathrm{d}\Gamma \tag{9}$$

with

$$\mathscr{W}^{\mathrm{aux}} = \int_0^{\varepsilon_{kl}^{\mathrm{aux}}} \sigma_{ij}^{\mathrm{aux}} \, \mathrm{d}\varepsilon_{ij}^{\mathrm{aux}}, \tag{10}$$

and M is the interaction integral involving the cross terms of actual and auxiliary fields, which is given by

$$M = \int_{\Gamma} \left\{ \frac{1}{2}(\sigma_{ik}\varepsilon_{ik}^{\mathrm{aux}} + \sigma_{ik}^{\mathrm{aux}}\varepsilon_{ik})\delta_{1j} - (\sigma_{ij} u_{i,1}^{\mathrm{aux}} + \sigma_{ij}^{\mathrm{aux}} u_{i,1}) \right\} n_j \, \mathrm{d}\Gamma. \tag{11}$$

The M-integral deals with interaction terms only, and will be used directly for solving mixed-mode fracture mechanics problems.

3.2. Auxiliary fields for T-stress

The auxiliary fields are judiciously chosen for the interaction integral depending on the nature of the problem to be solved. Since the T-stress is a constant stress that is parallel to the crack, the auxiliary stress and displacement fields are chosen due to a point force f in the x_1 direction (locally), applied to the tip of a semi-infinite crack in an infinite homogeneous body, as shown in Fig. 2(a).

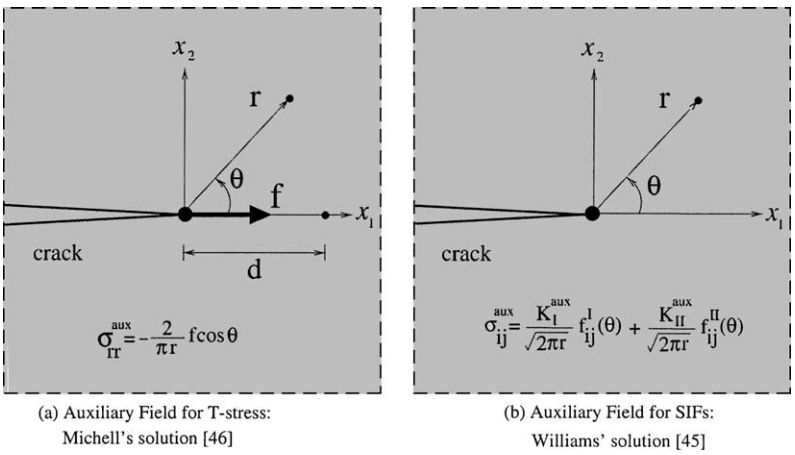

(a) Auxiliary Field for T-stress: Michell's solution [46]

(b) Auxiliary Field for SIFs: Williams' solution [45]

Fig. 2. The loading configuration of the auxiliary fields: (a) a point force applied to the crack in an infinite plate for T-stress computation [46]; (b) Williams' asymptotic solution for SIF computation [45].

The auxiliary stresses are given by Michell's solution [46]:

$$\sigma_{11}^{\text{aux}} = -\frac{f}{\pi r}\cos^3\theta, \qquad \sigma_{22}^{\text{aux}} = -\frac{f}{\pi r}\cos\theta\sin^2\theta, \qquad \sigma_{12}^{\text{aux}} = -\frac{f}{\pi r}\cos^2\theta\sin\theta. \tag{12}$$

The corresponding auxiliary displacements are [47]

$$u_1^{\text{aux}} = -\frac{f(1+\kappa)}{8\pi\mu}\ln\frac{r}{d} - \frac{f}{4\pi\mu}\sin^2\theta, \qquad u_2^{\text{aux}} = -\frac{f(\kappa-1)}{8\pi\mu}\theta + \frac{f}{4\pi\mu}\sin\theta\cos\theta \tag{13}$$

where d is the coordinate of a fixed point on the x_1 axis (see Fig. 2(a)), μ is the shear modulus, and

$$\kappa = \begin{cases} (3-\nu)/(1+\nu) & \text{plane stress} \\ (3-4\nu) & \text{plane strain.} \end{cases} \tag{14}$$

3.3. Determination of T-stress

By considering the auxiliary field in Eq. (12), a simple expression for the T-stress in terms of the interaction integral (M), the point force for the auxiliary field (f), and material properties (E, ν) can be obtained. Since the modulus of elasticity is same for both the actual and the auxiliary states, the stresses are

$$\sigma_{ij} = C_{ijkl}\varepsilon_{kl} \qquad \text{and} \qquad \sigma_{ij}^{\text{aux}} = C_{ijkl}\varepsilon_{kl}^{\text{aux}}, \tag{15}$$

where C_{ijkl} is the constitutive tensor. Then, from Eq. (15)

$$\sigma_{ij}\varepsilon_{kl}^{\text{aux}} = \sigma_{ij}^{\text{aux}}\varepsilon_{kl}. \tag{16}$$

Therefore, Eq. (11) can be rewritten as

$$M = \int_\Gamma \{(\sigma_{ik}\varepsilon_{ik}^{\text{aux}}\delta_{1j} - (\sigma_{ij}u_{i,1}^{\text{aux}} + \sigma_{ij}^{\text{aux}}u_{i,1})\}n_j\,\mathrm{d}\Gamma. \tag{17}$$

The M-integral is path-independent, and thus any arbitrary path can be chosen to evaluate the integral. The actual stress field is composed of singular terms, T-stress term and higher order terms (see Eqs. (1) and (3)). Considering a circular integration path, if Γ shrinks to zero ($r \to 0$), then the contribution of the higher order terms tends to zero. The coefficients of the singular terms $O(r^{-1/2})$ after the integration over θ from $-\pi$ to $+\pi$ in Eq. (17) sum to zero (see Appendix D). As a result, the only contribution to the M-integral comes from the T-stress term. Hence, the only stress to be considered is in the crack direction, i.e.

$$\sigma_{ij} = T\delta_{1i}\delta_{1j}, \tag{18}$$

or $\sigma_{11} = T$. By means of Eq. (18), the stress–strain and strain–displacement relationships are

$$u_{1,1} = \frac{T}{E'} \qquad \text{and} \qquad u_{1,1}^{\text{aux}} = \varepsilon_{11}^{\text{aux}}. \tag{19}$$

Thus, the first two terms of Eq. (17) cancel out and we get

$$M = -\lim_{\Gamma\to 0}\int_\Gamma \sigma_{ij}^{\text{aux}}n_j u_{i,1}\,\mathrm{d}\Gamma = -\frac{T}{E'}\lim_{\Gamma\to 0}\int_\Gamma \sigma_{ij}^{\text{aux}}n_j\,\mathrm{d}\Gamma. \tag{20}$$

In the auxiliary state, the force f is in equilibrium (see Fig. 2(a)), thus

$$f = -\lim_{\Gamma\to 0}\int_\Gamma \sigma_{ij}^{\text{aux}}n_j\,\mathrm{d}\Gamma, \tag{21}$$

and by substituting back into Eq. (20), we obtain

$$T = \frac{E'}{f}M \tag{22}$$

where

$$E' = \begin{cases} E & \text{plane stress} \\ E/(1-\nu^2) & \text{plane strain.} \end{cases} \tag{23}$$

By calculating the M-integral from Eq. (17) and plugging the value in Eq. (22), the T-stress can be readily obtained.

3.4. Auxiliary fields for SIFs

The mixed-mode SIFs can be extracted from the interaction integral, Eq. (11), through an appropriate definition of auxiliary fields. Local Cartesian and polar coordinates originate from the crack-tip (see Fig. 1). According to Fig. 2(b), the auxiliary stress fields (expressed in polar coordinates) are given by

$$\sigma_{ij}^{\text{aux}} = \frac{K_{\text{I}}^{\text{aux}}}{\sqrt{2\pi r}} f_{ij}^{\text{I}}(\theta) + \frac{K_{\text{II}}^{\text{aux}}}{\sqrt{2\pi r}} f_{ij}^{\text{II}}(\theta), \qquad (i,j = 1,2) \tag{24}$$

where the angular functions $f_{ij}(\theta)$ are given in Appendix A. The corresponding auxiliary displacement fields are given by

$$u_i^{\text{aux}} = \frac{K_{\text{I}}^{\text{aux}}}{\mu}\sqrt{\frac{r}{2\pi}}\, g_i^{\text{I}}(\theta) + \frac{K_{\text{II}}^{\text{aux}}}{\mu}\sqrt{\frac{r}{2\pi}}\, g_i^{\text{II}}(\theta), \tag{25}$$

$(i = 1,2)$

where μ is the shear modulus, and $K_{\text{I}}^{\text{aux}}$ and $K_{\text{II}}^{\text{aux}}$ are the auxiliary mode I and mode II SIFs, respectively. The angular functions $g_i(\theta)$ are also given in Appendix A. These angular functions can be found in many references on fracture mechanics, e.g. the textbook by Anderson [2] or Hills et al. [48].

3.5. Determination of SIFs

The relationship among the J-integral and the mode I and mode II stress intensity factors (SIFs) (K_{I} and K_{II}) is established as

$$J = \frac{K_{\text{I}}^2 + K_{\text{II}}^2}{E'} \tag{26}$$

where E' is given by Eq. (23). By superimposing the actual and auxiliary fields, and using Eq. (26), one obtains

$$J^{\text{s}} = \frac{(K_{\text{I}} + K_{\text{I}}^{\text{aux}})^2 + (K_{\text{II}} + K_{\text{II}}^{\text{aux}})^2}{E'} = J^{\text{aux}} + J + M \tag{27}$$

where

$$J^{\text{aux}} = \frac{(K_{\text{I}}^{\text{aux}})^2 + (K_{\text{II}}^{\text{aux}})^2}{E'} \tag{28}$$

and

$$M = \frac{2}{E'}(K_{\text{I}}K_{\text{I}}^{\text{aux}} + K_{\text{II}}K_{\text{II}}^{\text{aux}}). \tag{29}$$

The mode I SIF (K_{I}) is computed by assigning the SIFs of the auxiliary field to $K_{\text{I}}^{\text{aux}} = 1.0$ and $K_{\text{II}}^{\text{aux}} = 0.0$ in Eq. (29), i.e.

$$K_{\text{I}} = \frac{E'}{2} M \;\; (K_{\text{I}}^{\text{aux}} = 1.0,\; K_{\text{II}}^{\text{aux}} = 0.0). \tag{30}$$

Similarly, the mode II SIF (K_{II}) can be obtained by assigning $K_{\text{I}}^{\text{aux}} = 0.0$ and $K_{\text{II}}^{\text{aux}} = 1.0$ in Eq. (29), i.e.

$$K_{\text{II}} = \frac{E'}{2} M \;\; (K_{\text{I}}^{\text{aux}} = 0.0,\; K_{\text{II}}^{\text{aux}} = 1.0). \tag{31}$$

The M-integral in Eqs. (30) and (31) is evaluated by means of Eq. (11) and the auxiliary fields given by Eqs. (24) and (25).

4. Symmetric Galerkin boundary element method

The basic symmetric Galerkin BEM (SGBEM) framework for two-dimensional (2D) elastic boundary value problems is introduced in this section. First, the algorithm for bodies without cracks is provided. Then, the fracture algorithm is developed followed by a section on crack-tip elements.

4.1. Basic SGBEM formulation for 2D elasticity

The boundary integral equation (BIE) for a source point P interior to the domain for linear elasticity without body forces [49] is given by

$$u_k(P) - \int_{\Gamma_b} [U_{kj}(P,Q)\tau_j(Q) - T_{kj}(P,Q)u_j(Q)]\mathrm{d}Q = 0, \tag{32}$$

where Q is a field point, τ_j and u_j are traction and displacement vectors, respectively, U_{kj} and T_{kj} are the Kelvin kernel tensors and Γ_b denotes the boundary of the domain.

For plane strain problems (see, e.g. Ref. [49]), the Kelvin kernels are

$$U_{kj} = \frac{1}{8\pi G(1-\nu)}[r_{,k}r_{,j} - (3-4\nu)\delta_{kj}\ln(r)], \tag{33}$$

$$T_{kj} = -\frac{1}{4\pi(1-\nu)r}\left[\{(1-2\nu)\delta_{kj} + 2r_{,k}r_{,j}\}\frac{\partial r}{\partial n} - (1-2\nu)(n_j r_{,k} - n_k r_{,j})\right], \tag{34}$$

where ν is Poisson's ratio, G is shear modulus, δ_{ij} is the Kronecker delta and

$$r_k = x_k(Q) - x_k(P), \qquad r^2 = r_i r_i, \qquad r_{,k} = r_k/r \quad \text{and} \quad \partial r/\partial n = r_{,i}n_i. \tag{35}$$

For a point P interior to the domain, the displacement gradient can be obtained by differentiating Eq. (32) with respect to the source point P. As P approaches the boundary, the limit of right-hand-side of Eq. (32) exists [25]. For $P \in \Gamma_b$, the BIE is defined in the limiting sense. Substituting the displacement gradient into the Hooke's law, we get

the HBIE for the boundary stresses

$$\sigma_{kl}(P) - \int_{\Gamma_b} [D_{kjl}(P,Q)\tau_j(Q) - S_{kjl}(P,Q)u_j(Q)]\mathrm{d}Q = 0, \tag{36}$$

where the kernels are given by [49]

$$D_{kjl} = \frac{1}{4\pi(1-\nu)r}[(1-2\nu)(\delta_{kj}r_{,l} + \delta_{jl}r_{,k} - \delta_{lk}r_{,j}) + 2r_{,k}r_{,j}r_{,l}], \tag{37}$$

$$S_{kjl} = \frac{G}{2\pi(1-\nu)r^2}\Big[2\frac{\partial r}{\partial n}\{(1-2\nu)\delta_{lk}r_{,j} + \nu(\delta_{kj}r_{,l} + \delta_{jl}r_{,k}) - 4r_{,k}r_{,j}r_{,l}\} + 2\nu(n_k r_{,j} r_{,l} + n_l r_{,k} r_{,j}) + (1-2\nu)(2n_j r_{,l} r_{,k} + \delta_{kj}n_l + \delta_{jl}n_k) - (1-4\nu)\delta_{lk}n_j\Big]. \tag{38}$$

In the collocation approach, the BIE (32) and HBIE (36) are enforced at discrete source points. In a Galerkin approximation, the error in the approximate solution is orthogonalized against the shape functions. The shape functions are the weighting functions and the integral equations (32) and (36) are enforced in the 'weak sense', i.e.

$$\int_{\Gamma_b} \psi_m(P)\Big[u_k(P) - \int_{\Gamma_b} [U_{kj}(P,Q)\tau_j(Q) - T_{kj}(P,Q) \times u_j(Q)]\mathrm{d}Q\Big]\mathrm{d}P = 0, \tag{39}$$

$$\int_{\Gamma_b} \psi_m(P)\Big[\sigma_{kl}(P) - \int_{\Gamma_b} [D_{kjl}(P,Q)\tau_j(Q) - S_{kjl}(P,Q)u_j(Q)]\mathrm{d}Q\Big]\mathrm{d}P = 0, \tag{40}$$

respectively. As a result, the Galerkin technique possesses the important property of the *local support*. A symmetric coefficient matrix in the symmetric-Galerkin approximation can be obtained by using Eq. (39) on the boundary $\Gamma_{b(\mathbf{u})}$ where displacements u_{bv} are prescribed, and using Eq. (40) on the boundary $\Gamma_{b(\boldsymbol{\tau})}$ with prescribed tractions τ_{bv} (see Fig. 3). Note that, $\Gamma_b = \Gamma_{b(\mathbf{u})} + \Gamma_{b(\boldsymbol{\tau})}$ for a well-posed boundary value problem.

The additional boundary integration is the key to obtaining a symmetric coefficient matrix, as this ensures

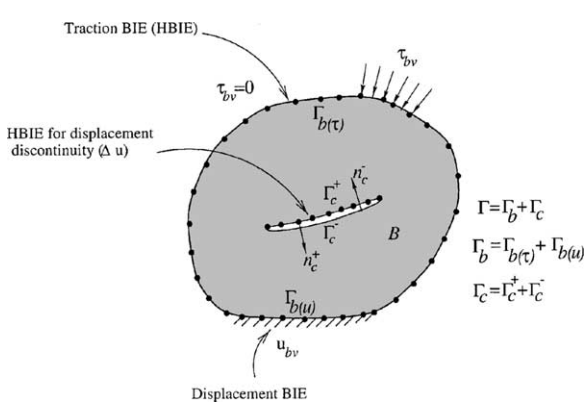

Fig. 3. Configuration of the fracture scheme using the SGBEM. Notice that on the crack surface, only the upper surface is discretized and the unknown is the displacement discontinuity. The bullets denote the nodal points.

that the source point P and field point Q are treated in the same manner in evaluating the kernel tensors U_{kj}, T_{kj}, D_{kjl} and S_{kjl}. After discretization, the resulting equation system can be written in block-matrix form [25] as

$$\begin{bmatrix} H_{11} & H_{12} \\ H_{21} & H_{22} \end{bmatrix}\begin{Bmatrix} u_{bv} \\ u_* \end{Bmatrix} = \begin{bmatrix} G_{11} & G_{12} \\ G_{21} & G_{22} \end{bmatrix}\begin{Bmatrix} \tau_* \\ \tau_{bv} \end{Bmatrix}. \tag{41}$$

Here, the first and second rows represent, respectively, the BIE written on $\Gamma_{b(\mathbf{u})}$ and the HBIE written on $\Gamma_{b(\boldsymbol{\tau})}$. Further, u_* and τ_* denote unknown displacement and traction vectors. Rearranging Eq. (41) into the form $[A]\{x\} = \{b\}$, and multiplying the HBIE by -1, one obtains

$$\begin{bmatrix} -G_{11} & H_{12} \\ G_{21} & -H_{22} \end{bmatrix}\begin{Bmatrix} \tau_* \\ u_* \end{Bmatrix} = \begin{Bmatrix} -H_{11}u_{bv} + G_{12}\tau_{bv} \\ H_{21}u_{bv} - G_{22}\tau_{bv} \end{Bmatrix} \tag{42}$$

The symmetry of the coefficient matrix, $G_{11} = G_{11}^{\mathrm{T}}$, $H_{22} = H_{22}^{\mathrm{T}}$, and $H_{12} = G_{21}^{\mathrm{T}}$ now follows from the symmetry properties of the kernel tensors [25].

4.2. Fracture analysis with the SGBEM

The symmetric-Galerkin formulation for linear elastic fracture analysis is provided in this section. Consider a body of arbitrary shape B which contains a crack, as shown in Fig. 3. The boundary Γ of the body B is composed of non-crack boundary Γ_b and the crack surface Γ_c. The portion of the boundary Γ_b with prescribed displacements is denoted by $\Gamma_{b(\mathbf{u})}$, and the portion with prescribed traction boundary is denoted by $\Gamma_{b(\tau)}$. The crack surface Γ_c consists of two coincident surfaces Γ_c^+ and Γ_c^-, where Γ_c^+ and Γ_c^- represent the upper and lower crack surfaces, respectively. The outward normals to the crack surfaces, designated by n_c^+ and n_c^- are oriented in opposite directions and at any point on the crack $n_c^- = -n_c^+$ (see Fig. 3). On the crack surface, it is assumed that only traction is specified. Therefore, the traction HBIE is applied on the crack surface boundaries. Since the only difference between the two coincident crack surfaces is the orientation of the normals ($n_c^- = -n_c^+$), it is convenient to replace the displacements $\mathbf{u}_c^+$ and $\mathbf{u}_c^-$ by the single crack opening displacement $\Delta\mathbf{u}_c = \mathbf{u}_c^+ - \mathbf{u}_c^-$, and the tractions τ_c^+ and τ_c^- by the sum of tractions $\sum\tau_c = \tau_c^+ + \tau_c^-$. As a consequence, it suffices to discretize the upper crack surface Γ_c^+. Thus, the BIE and HBIE written for an interior point P take the following form:

$$u_k(P) = \int_{\Gamma_b} [U_{kj}(P,Q)\tau_j(Q) - T_{kj}(P,Q)u_j(Q)]\mathrm{d}Q + \int_{\Gamma_c^+} [U_{kj}(P,Q)\sum\tau_j(Q) - T_{kj}(P,Q)\Delta u_j(Q)]\mathrm{d}Q, \tag{43}$$

$$\sigma_{kl}(P) = \int_{\Gamma_b} [D_{lkm}(P,Q)\tau_m(Q) - S_{lkm}(P,Q)u_m(Q)]\mathrm{d}Q + \int_{\Gamma_c^+} [D_{lkm}(P,Q)\sum\tau_m(Q) - S_{lkm}(P,Q)\Delta u_m(Q)]\mathrm{d}Q. \tag{44}$$

However, since the crack surfaces are usually symmetrically loaded, i.e. $\tau_c^- = -\tau_c^+$, one gets

$$u_k(P) = \int_{\Gamma_b} [U_{kj}(P,Q)\tau_j(Q) - T_{kj}(P,Q)u_j(Q)]\mathrm{d}Q - \int_{\Gamma_c^+} T_{kj}(P,Q)\Delta u_j(Q)\mathrm{d}Q, \tag{45}$$

$$\sigma_{kl}(P) = \int_{\Gamma_b} [D_{lkm}(P,Q)\tau_m(Q) - S_{lkm}(P,Q)u_m(Q)]\mathrm{d}Q - \int_{\Gamma_c^+} S_{lkm}(P,Q)\Delta u_m(Q)]\mathrm{d}Q. \tag{46}$$

Previous boundary element solutions of fracture mechanics problems in terms of displacement discontinuities have been presented by Crouch and co-workers [50,51]. In the Galerkin approximation for the non-crack boundary Γ_b, the limit of Eqs. (45) and (46) is taken as $P \to \Gamma_{b(\mathbf{u})}$ and $\Gamma_{b(\tau)}$, respectively. Since tractions are prescribed on the crack surface Γ_c^+, only Eq. (46) is written for source points on Γ_c^+ and, following the Galerkin approximation, the limit of Eq. (46) as $P \to \Gamma_c^+$ is considered. Converting the stress equation (46) into a traction equation through the identity $\tau_k(P) = \sigma_{lk}(P)n_l(P)$, with $n_l(P)$ being the outward normal at P and discretizing, the following system is obtained from Eqs. (45) and (46) in block matrix form

$$\begin{bmatrix} H_{bb} & H_{bc} \\ H_{cb} & H_{cc} \end{bmatrix} \begin{Bmatrix} u_b \\ \Delta u_c \end{Bmatrix} = \begin{bmatrix} G_{bb} & 0 \\ G_{cb} & G_{cc} \end{bmatrix} \begin{Bmatrix} \tau_b \\ -\tau_c^+ \end{Bmatrix}, \tag{47}$$

where the subscripts b and c denote the contribution of the non-crack boundary and upper crack surface, respectively. For the present case, with traction free cracks ($\tau_c = 0$), the system of equations reduces to

$$\begin{bmatrix} H_{bb} & H_{bc} \\ H_{cb} & H_{cc} \end{bmatrix} \begin{Bmatrix} u_b \\ \Delta u_c \end{Bmatrix} = \begin{bmatrix} G_{bb} & 0 \\ G_{cb} & G_{cc} \end{bmatrix} \begin{Bmatrix} \tau_b \\ 0 \end{Bmatrix}. \tag{48}$$

The vector τ_b is a mixture of known traction τ_{bv} and unknown traction τ_*, similarly u_b is a mixture of known displacement u_{bv} and unknown displacement u_*. Eq. (48) can be written in terms of the known and unknown boundary displacement and traction values as

$$\begin{bmatrix} H_{b_u b_u} & H_{b_u b_\tau} & H_{b_u c} \\ H_{b_\tau b_u} & H_{b_\tau b_\tau} & H_{b_\tau c} \\ H_{c b_u} & H_{c b_\tau} & H_{cc} \end{bmatrix} \begin{Bmatrix} u_{bv} \\ u_* \\ \Delta u_c \end{Bmatrix} = \begin{bmatrix} G_{b_u b_u} & G_{b_u b_\tau} & 0 \\ G_{b_\tau b_u} & G_{b_\tau b_\tau} & 0 \\ G_{c b_u} & G_{c b_\tau} & G_{cc} \end{bmatrix} \begin{Bmatrix} \tau_* \\ \tau_{bv} \\ 0 \end{Bmatrix}, \tag{49}$$

where the subscripts b_u, b_τ and c represents the terms corresponding to the non-crack boundary with prescribed displacements $\Gamma_{b(\mathbf{u})}$, non-crack boundary with prescribed tractions $\Gamma_{b(\boldsymbol{\tau})}$ and the crack surface Γ_c^+, respectively. By rearranging Eq. (49) into the form $[A]\{x\} = \{b\}$, and multiplying the HBIEs by -1, we get the system of the matrix

$$\begin{bmatrix} -G_{b_u b_u} & H_{b_u b_\tau} & H_{b_u c} \\ G_{b_\tau b_u} & -H_{b_\tau b_\tau} & -H_{b_\tau c} \\ G_{c b_u} & -H_{c b_\tau} & -H_{cc} \end{bmatrix} \begin{Bmatrix} \tau_* \\ u_* \\ \Delta u_c \end{Bmatrix} = \begin{Bmatrix} -H_{b_u b_u} u_{bv} + G_{b_u b_\tau} \tau_{bv} \\ H_{b_\tau b_u} u_{bv} - G_{b_\tau b_\tau} \tau_{bv} \\ H_{c b_u} u_{bv} - G_{c b_\tau} \tau_{bv} \end{Bmatrix}. \tag{50}$$

The final coefficient matrix of this system is symmetric due to the symmetric properties of the kernel tensors [25,52]. Further details can be found in Refs. [24,25,52–54].

4.3. Crack-tip elements

In fracture analysis, a quarter-point element at the crack-tip accounts for the $\sqrt{r}$ displacement behaviour of the crack-tip, where r is the distance from the source point to the tip. The quarter-point element is formed from the standard quadratic element by simply moving the mid-node coordinates three-fourths of the way towards the crack-tip [55,56] (see Fig. 4). The modified quarter-point (MQP) crack-tip element [26] is based on the standard quarter-point element, but altered to account for a constraint on the linear term as suggested by Gray and Paulino [57]. This constraint is implemented in the modified shape functions by including a cubic term. Use of this element has been shown to greatly improve the accuracy in computed values for SIFs by means of local techniques [26]. The present algorithm makes use of all the crack-tip elements shown in Fig. 4.

The standard quadratic shape functions are defined in terms of the intrinsic coordinate $t \in [0,1]$ by

$$\psi_1(t) = (1-t)(1-2t), \qquad \psi_2(t) = 4t(1-t), \qquad \psi_3(t) = t(2t-1) \tag{51}$$

and thus the boundary interpolation is

$$\Gamma(t) = \sum_{j=1}^{3} (x_j\psi_j(t), y_j\psi_j(t)). \tag{52}$$

For the standard quarter-point crack-tip element, shown in Fig. 4, the mid-side node is moved to the quarter-point position. The effect of this is that $t \approx \sqrt{(r)}$, which provides the singular behavior at the tip. For the modified quarter-point, the displacement discontinuity is given by

$$\Delta\mathbf{u}(t) = \sum_{j=2}^{3} (\Delta u_1^j \hat{\psi}_j(t), \Delta u_2^j \hat{\psi}_j(t)), \tag{53}$$

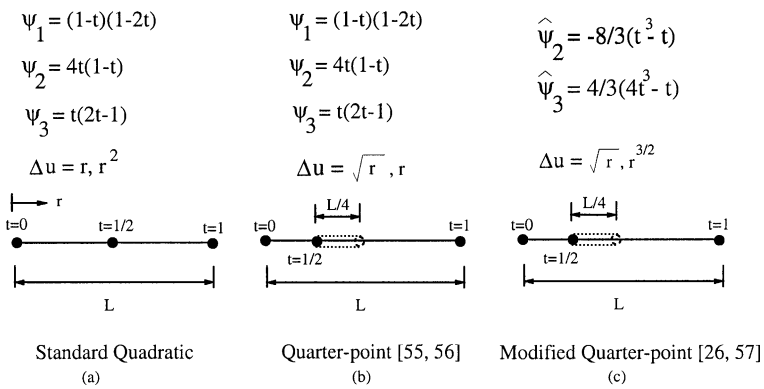

Fig. 4. The shape functions, positions of the nodes and order of the crack opening displacement function for standard quadratic, quarter-point and the modified quarter-point element are shown.

where the new shape functions $\hat{\psi}$ are

$$\hat{\psi}_2(t) = 4t(1-t) - 4t(1-t)(1-2t)/3 = -8(t^3 - t)/3,$$
$$\hat{\psi}_3(t) = t(2t-1) + 2t(1-t)(1-2t)/3 = (4t^3 - t)/3. \tag{54}$$

As the intrinsic coordinate t is proportional to $\sqrt{r}$, the MQP element is seen to give crack opening displacements which are of the form $\Delta u_k = A\sqrt{r} + Br^{3/2}$; the absence of the linear term in r is consistent with the proof by Gray and Paulino [57]. It should be noted that the shape function $\hat{\psi}_1(t)$ is not defined, as it multiplies the crack opening displacement at the tip which is known to be zero.

4.4. Numerical implementation of the M-integral

The accuracy of the computation of the M-integral depends on the integration points of the path and the method of integration. Integrals are evaluated along the circular path centered at the crack-tip as shown in Fig. 5.

The integration along the contour path can be performed by using simple trapezoidal rule or Gaussian quadrature formula. The contour integrals can be written as follows

$$M = \int_{\Gamma_i} F_N(x,y)\mathrm{d}\Gamma_i, \qquad (x,y)\epsilon\Gamma \tag{55}$$

where F_N denotes the integrand of Eq. (11) and Γ_i is the integration path of interest. The following formula is used for the trapezoidal rule

$$\int_{\Gamma_i} F_N(x,y)\mathrm{d}\Gamma_i = \frac{\pi}{m}\sum_{n=1}^{2m} F_N\left(h\cos\frac{\pi n}{m}, h\sin\frac{\pi n}{m}\right) \tag{56}$$

where h is the radius of the circular path. Alternatively Eq. (55) in polar (r,ω) coordinates is given by

$$M = h\int_{-\pi}^{\pi} F_N(r,\omega)\mathrm{d}\omega. \tag{57}$$

In order to use the Gaussian–Legendre quadrature rule, Eq. (57) is written as

$$M = h\pi\int_{-1}^{1} F_N(r,\pi s)\mathrm{d}s. \tag{58}$$

Convergence is achieved by using 30 or more integration points for the trapezoidal rule and eight or more integration points for the Gauss–Legendre rule. For the numerical examples presented in this paper, the Gaussian integration scheme is used.

5. Numerical examples

The performance of the M-integral method for extracting SIFs and T-stress is examined by means of numerical examples. In order to assess the various features of the method, the following examples are presented.

(1) Infinite plate with an interior inclined crack.
(2) Slanted edge crack in a finite plate.
(3) Multiple interacting cracks.

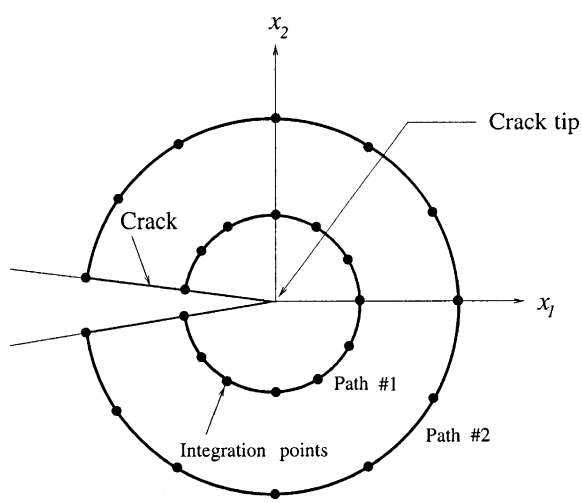

Fig. 5. Integration contours for evaluation of the M-integral.

(4) Fracture specimen configurations.
- Single edge notch tension (SENT) specimen.
- Single edge notch bending (SENB) specimen.
- Center cracked tension (CCT) or middle crack tension (MT) specimen.
- Double edge notched tension (DENT) specimen.

The first example is an inclined central crack in an infinite plate. This problem has analytical solution for both T-stress and SIFs. An edge crack in a finite plate is analysed in the second problem and compared with reference solutions. The third problem is an interesting problem consisting of two interacting cracks in a finite plate. The last example investigates the benchmark examples as used for laboratory experiments and provides solution for the T-stress, SIF and the associated biaxiality ratios. Unless otherwise stated, in all the examples we use modified quarter-point element at the crack-tips.

5.1. Infinite plate with an interior inclined crack

Consider a plate containing a single interior crack of length $2a$ oriented at an angle θ with the horizontal direction as shown in Fig. 6. The plate is loaded with a uniform far-field traction $\sigma = 1$ applied symmetrically in the vertical direction and $\lambda\sigma$ in the horizontal direction, where λ is the lateral load ratio. The crack length is $2a = 2$ and the plate dimensions are $2H = 2W = 100$, which can be considered as an infinite domain. T-stress, K_{I} and K_{II} are calculated for various values of θ where $0 < \theta < \pi/2$. The boundary of the plate is discretized with only two quadratic elements on each side, and the crack is discretized with four elements. The number of Gauss points used for integration is $n = 8$. The Young's modulus is taken as $E = 1.0$ (consistent units) and Poisson's ratio is $\nu = 0.3$. The exact solutions of

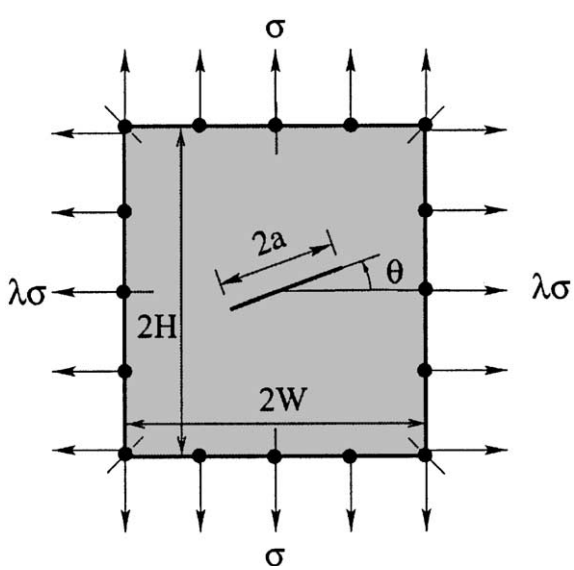

Fig. 6. A single interior inclined crack in a plate subject to biaxial loading. The outer boundary of the plate is discretized with only two quadratic elements on each edge.

Table 1
T-stress and normalized SIFs as functions of the crack angle θ for the lateral load ratio $\lambda = 0$

Angle θ (°)	SGBEM (M-integral)			Analytical solution		
	$K_{\mathrm{I}}/\sqrt{\pi a}$	$K_{\mathrm{II}}/\sqrt{\pi a}$	T	$K_{\mathrm{I}}/\sqrt{\pi a}$	$K_{\mathrm{II}}/\sqrt{\pi a}$	T
0	1.0002	0.0000	−1.0013	1.0000	0.0000	−1.0000
15	0.9332	0.2502	−0.8672	0.9330	0.2500	−0.8660
30	0.7502	0.4334	−0.5009	0.7500	0.4330	−0.5000
45	0.5001	0.5004	−0.0006	0.5000	0.5000	0.0000
60	0.2500	0.4333	0.4997	0.2500	0.4330	0.5000
75	0.0670	0.2502	0.8659	0.0670	0.2500	0.8660
90	0.0000	0.0000	1.0000	0.0000	0.0000	1.0000

the SIFs and the T-stress for this problem [5] are

$$K_{\mathrm{I}} = \sigma(\lambda \sin^2\theta + \cos^2\theta)\sqrt{\pi a}$$
$$K_{\mathrm{II}} = \sigma(1-\lambda)\cos\theta\sin\theta\sqrt{\pi a} \tag{59}$$
$$T = -(1-\lambda)\sigma\cos 2\theta.$$

The results of T-stress, normalized K_{I} and K_{II} for the right crack-tip and the corresponding analytical solution for $\lambda = 0$ (uniaxially loaded) and $\lambda = 0.5$ (biaxially loaded) are presented in Tables 1 and 2, respectively. The results show good agreement between numerical (SGBEM) and analytical (Eq. (59)) results.

The influence of several parameters, i.e. the radius of the integration contour r, the number of integration points n, crack discretization m, and the crack-tip elements on the calculated SIFs and the T-stress is studied next using the SGBEM.

5.1.1. Effect of the radius of the integration contour

The M-integral is evaluated along different circular integration paths as shown in Fig. 5. The K_{I}, K_{II} and T-stress results are obtained for several circular paths at the right crack-tip with the radius of the circular contour r ranging from $r = 0.025a$ (near crack-tip) to $r = 1.5a$ (closer to opposite crack-tip). According to Fig. 6, the crack angle is $\theta = 30°$, and the lateral load ratio is $\lambda = 0$. The outer boundary of the plate is discretized with only two quadratic

Table 2
T-stress and normalized SIFs as function of the crack angle θ for the lateral load ratio $\lambda = 0.5$

Angle θ (°)	SGBEM (M-integral)			Analytical solution		
	$K_{\mathrm{I}}/\sqrt{\pi a}$	$K_{\mathrm{II}}/\sqrt{\pi a}$	T	$K_{\mathrm{I}}/\sqrt{\pi a}$	$K_{\mathrm{II}}/\sqrt{\pi a}$	T
0	1.0003	0.0000	−0.5011	1.0000	0.0000	−0.5000
15	0.9668	0.1251	−0.4341	0.9665	0.1250	−0.4330
30	0.8752	0.2167	−0.2509	0.8750	0.2165	−0.2500
45	0.7502	0.2502	0.0007	0.7500	0.2500	0.0000
60	0.6251	0.2167	0.2494	0.6250	0.2165	0.2500
75	0.5336	0.1251	0.4324	0.5335	0.1250	0.4300
90	0.5001	0.0000	0.4994	0.5000	0.0000	0.5000

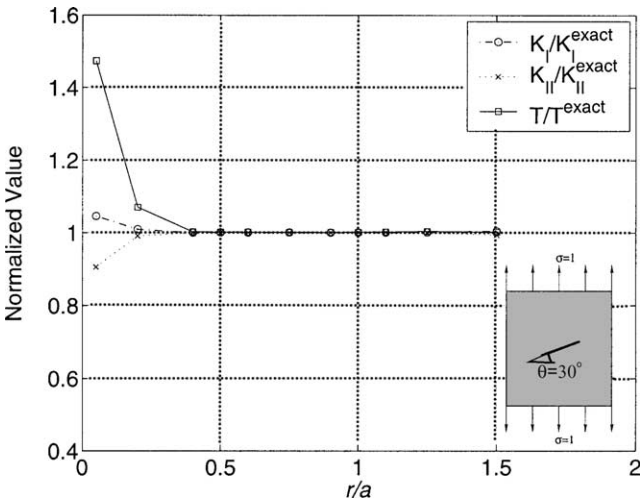

Fig. 7. Variation of normalized SIFs and T-stress with different values of r/a. Parameters adopted: $\theta = 30°$, $\lambda = 0$, $m = 10$, $n = 8$.

elements on each side. The crack is discretized with 10 elements since smaller values of r/a are used. The number of Gauss points for integration is $n = 8$. A plot of normalized K_I, K_{II} and T-stress versus r/a is plotted in Fig. 7, which verifies the path independence of the integral. However, notice that the T-stress results are more sensitive to the radius of integration (r/a) than the SIFs.

5.1.2. Effect of the number of integration points in the contour

A convergence study with respect to the number of Gauss integration points (n) is carried out. The SIFs and T-stress are calculated and normalized values are plotted against n in Fig. 8 for n ranging from 6 to 20. According to Fig. 6, the crack angle is $\theta = 30°$ and the lateral load ratio is $\lambda = 0.5$. The outer boundary of the plate is discretized with only two quadratic elements on each side, the crack is discretized

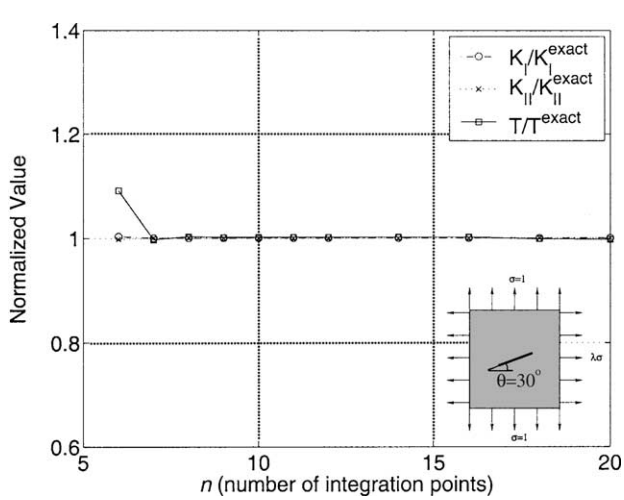

Fig. 8. Normalized SIFs and T-stress versus number of integration points (n) on the contour. Parameters adopted: $\theta = 30°$, $\lambda = 0.5$, $m = 10$, $r/a = 1.0$.

with 10 elements and $r/a = 1.0$. Fig. 8 shows that the results converge when n is equal to or greater than 8. The T-stress results are more sensitive to the number of integration points (n) than the SIFs. For higher values of n (e.g. $n > 20$), stress results at integration points very close to the crack face are required. Accurate stress evaluation close to the boundary requires appropriate treatment of near-singular integrals. In the present implementation, no special treatment has been considered for this purpose. Instead, by increasing the number of elements to discretize the crack (m), accurate results are obtained when n is large. However, for all the other problems presented in this paper the number of integration points n used was between 8 and 12, which proved sufficient.

5.1.3. Effect of crack discretization

A convergence study on crack discretization with the number of the elements on the crack m ranging from 2 to 14 elements is done. The crack is oriented at $\theta = 30°$ and $\lambda = 0.5$. The outer boundary of the plate is discretized with only two quadratic elements on each side. The number of Gauss points is $n = 8$. The normalized values of K_I/K_{II}^{exact}, K_{II}/K_{II}^{exact} and T/T^{exact} are presented in Table 3, which shows that discretizing the crack with four elements is sufficient for the present problem.

5.1.4. Effect of crack-tip elements

The influence of the type of crack-tip elements on the SIFs and the T-stress results is studied. The crack angle is $\theta = 30°$ and the lateral load ratio is $\lambda = 0.5$. The outer boundary of the plate is discretized with only two quadratic elements on each side and the crack is discretized with six elements. The number of Gauss points is $n = 8$ and $r/a = 1.0$. Table 4 shows normalized SIFs and the T-stress obtained by using standard quadratic elements (Fig. 4(a)), quarter-point elements (Fig. 4(b)) and modified quarter-point elements (Fig. 4(c)) as crack-tip elements. As expected, there is no significant difference in the results, especially for the latter two elements. Since the M-integral

Table 3
Effect of the crack discretization

m	K_I/K_I^{exact}	K_{II}/K_{II}^{exact}	T/T^{exact}
2	0.9982	0.9992	1.0621
3	0.9913	1.0075	1.0774
4	1.0002	1.0009	1.0043
5	1.0001	1.0010	1.0035
6	1.0002	1.0009	1.0036
7	1.0003	1.0014	1.0033
8	1.0003	1.0005	1.0034
9	1.0003	0.9997	1.0034
10	1.0003	1.0009	1.0034
11	1.0003	0.9992	1.0034
12	1.0003	1.0013	1.0034
14	1.0003	1.0004	1.0034

The parameter m denotes the number of elements on the crack surface.

Table 4
Effect of crack-tip elements on normalized SIFs and T-stress

Element type	$K_I/\sqrt{\pi a}$	$K_{II}/\sqrt{\pi a}$	T-stress
Quadratic (no quarter-point)	0.8737	0.2164	−0.2509
Quarter−point	0.8752	0.2167	−0.2509
Modified quarter-point	0.8752	0.2167	−0.2509
Analytical solution	0.8750	0.2165	−0.2500

is computed away from the crack-tip, the details of the local crack-tip interpolation do not have much influence on the results. However, such details are relevant for a local method like the DCT [26].

5.2. Slanted edge crack in a finite plate

Fig. 9 shows a slanted edge crack in a finite plate loaded with a uniform traction $\sigma = 1$ applied symmetrically at the ends. The crack length is $a/W = 0.4\sqrt{2}$ and the plate dimensions are $H = 2W = 1$ (consistent units). T-stress, K_I and K_{II} are calculated for the crack angle $\theta = 45°$. The outer boundary of the plate is discretized using 20 quadratic elements on the left side and 10 quadratic elements on rest of the sides. The crack is discretized using six elements ($m = 6$). The number of Gauss points is $n = 10$, and $r/a = 0.5$. The Young's modulus is taken as $E = 1.0$ (consistent units) and Poisson's ratio is $\nu = 0.3$. Kim and Paulino solved this problem previously using FEM by the J_k-integral [58] and the interaction integral [35]. Table 5 shows a comparison of the present results with those obtained in Refs. [35,58], which indicates good agreement.

5.3. Multiple interacting cracks

Fig. 10 shows two cracks of length $2a$ oriented with an angle θ_i ($\theta_1 = 30°$, $\theta_2 = 60°$) in a finite 2D plate. The distance from the origin of the coordinate system (see Fig. 10) to the two crack-tips which are closer to the origin is

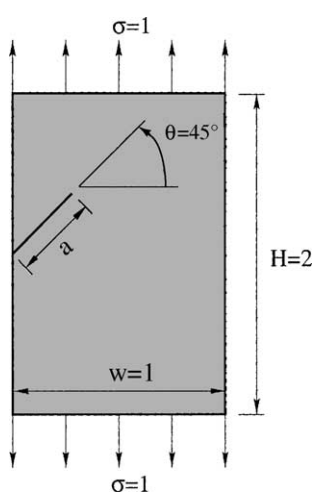

Fig. 9. Slanted edge crack in a plate.

Table 5
Comparison of normalized SIFs and T-stress

Method	$K_I/\sqrt{\pi a}$	$K_{II}/\sqrt{\pi a}$	T-stress
M-integral (present SGBEM)	1.446	0.615	0.775
J_k-integral [58]	1.451	0.604	0.787
M-integral [35]	1.446	0.615	0.764

1.0. Kim and Paulino [58] have provided finite element solution and Shbeeb et al. [59] have provided semi-analytical solutions using integral equation method for this problem. The applied load is $\sigma = 1.0$, the crack length is $2a = 2$, the plate dimensions are given by $H/W = 1.0$, $W = 20$, and the material properties are $E = 1.0$, $\nu = 0.0$ (consistent units). The number of integration point is $n = 12$ and $r/a = 1$. The outer boundary is discretized with 10 quadratic elements, and each of the cracks is discretized with 10 elements ($m = 10$). Table 6 shows a comparison of the normalized SIFs at crack-tips for the lower crack oriented at an angle $\theta = 30°$ computed by the present interaction integral (M) with those obtained using the J_k-integral [58] and the integral equation method [59]. Here, a^- and a^+ refer to the left and right crack-tips, respectively, in Table 6. The present results (SGBEM) agree very well with those by Kim and Paulino [58] and Shbeeb et al. [59].

5.4. Various fracture specimen configurations

This final example investigates the T-stress and the SIFs for various benchmark fracture specimens, i.e. CCT or MT specimen, the SENT specimen, the SENB specimen, and the DENT specimen as shown in Fig. 11. In order to understand the behaviour of the M-integral a plot of the integrand along the integration path ω from $-\pi$ to $+\pi$ for the SENT specimen with $a/W = 0.5$ is depicted in Fig. 12.

The analyses were carried out using plane strain conditions with Young's modulus $E = 1.0$ and Poisson's ratio $\nu = 0.3$. The applied load is $\sigma = 1$ for the different load configurations of Fig. 11 (consistent units). The crack is discretized using 10 elements ($m = 10$). The number of

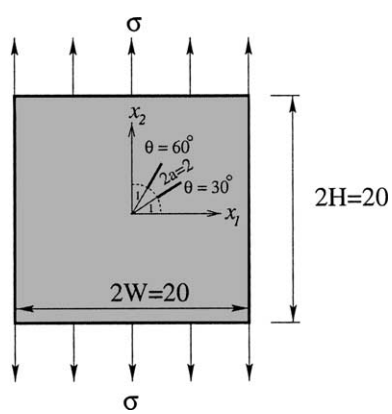

Fig. 10. Two interacting cracks in a plate.

Table 6
Comparison of the normalized SIFs for the lower crack among various methods

Method	$K_I(a^-)/\sqrt{\pi a}$	$K_{II}(a^-)/\sqrt{\pi a}$	$K_I(a^+)/\sqrt{\pi a}$	$K_{II}(a^+)/\sqrt{\pi a}$
M-integral (present SGBEM)	0.601	0.430	0.808	0.433
J_k-integral [58]	0.603	0.431	0.801	0.431
Integral equation [59]	0.59	0.43	0.78	0.42

Gauss integration point is $n = 10$. The outer boundary of the CCT specimen is discretized with 10 quadratic elements on each side, while for the rest of the specimens (SENT, SENB and DENT), the outer boundary is discretized with 50 quadratic elements on the left edge and 30 quadratic elements on the rest of the edges. Only half of the DENT specimen was analysed due to its symmetry. Table 7 shows good agreement between present results (SGBEM) and those available in the literature. Fig. 13 shows the variation of biaxiality ratio ($B = T\sqrt{\pi a}/K_I$) versus the ratio of crack length to width a/W for various specimens ($H/W = 12$) and compares with the results published by Fett et al. [60] using

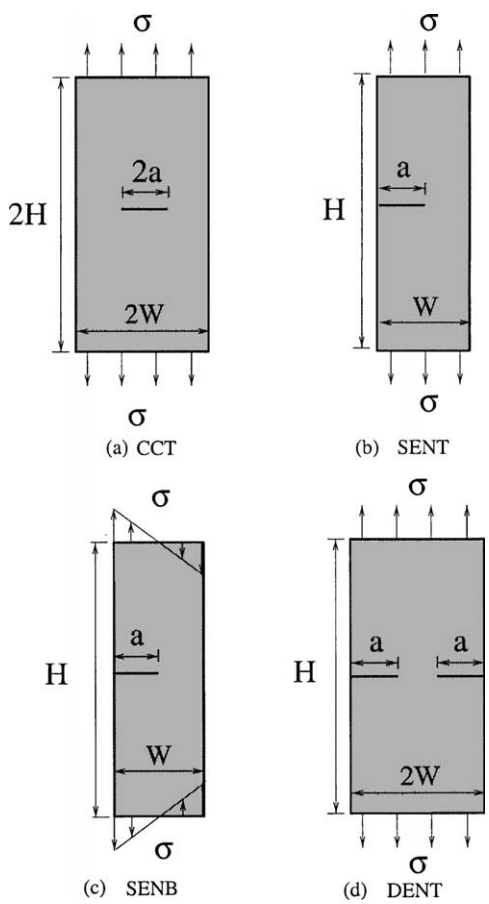

Fig. 11. Various fracture specimen configurations. The thickness of each specimen is t.

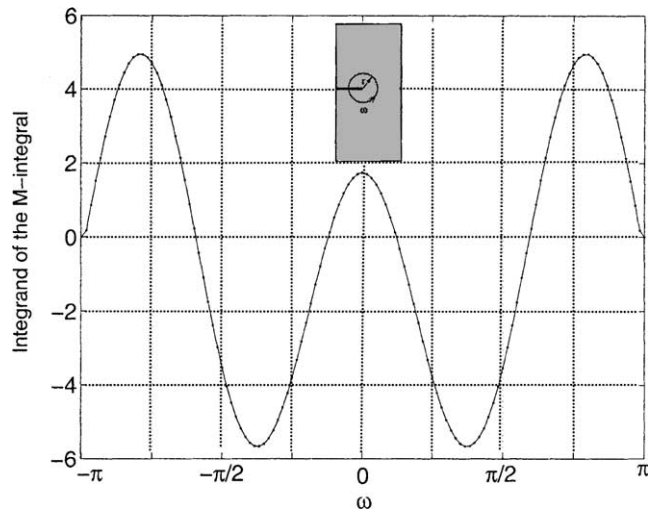

Fig. 12. Variation of integrand of the M-integral along the integration path ω with $r/a = 0.5$ where a is the crack length. Parameters adopted: $m = 10$, $n = 10$.

the boundary collocation method, and by Kim and Paulino [36] using the FEM. Notice that, for the SENB the present solution (SGBEM) is closer to that by Fett et al. [60], while, for the DENT, the present solution (SGBEM) is closer to that by Kim and Paulino [36]. In general, all the solutions (SGBEM, Fett et al. [60], and Kim and Paulino [36]) show very good agreement in Fig. 13. The sign of the biaxiality ratio changes from negative to positive as a/W increases in SENT and SENB, while the sign remains the same for CCT and DENT specimens.

6. Concluding remarks and extensions

The interaction integral method applied to mixed-mode crack problems to evaluate T-stress and the SIFs using the SGBEM has been presented. This method provides an accurate and robust scheme for calculating the fracture parameters. The numerical results obtained are in remarkable agreement with known results for single and multiple cracks. In general, the T-stress computations are more demanding than those for SIFs (see Figs. 7 and 8). This observation is in agreement with analogous studies in the FEM field—see for example Refs. [36,61].

The influence of several parameters on the SIFs and T-stress has been investigated, including the radius of the integration contour (r), the number of integration points (n), number of elements on the crack surface (m), and type of crack-tip elements. Based on the experience acquired with the present study, the number of Gauss points $n \geq 12$ and number of crack elements $m \geq 10$ give accurate results for all the problems investigated. A value of $r/a > 0.3$ is sufficient for most problems, except when a/W is large, where a is the length of the crack and W is the width of the plate. A fracture criteria which includes the SIFs and T-stress

Table 7
Normalized T-stress, biaxiality ratio (B), and normalized mode I SIF for various fracture specimens

Fracture specimen	Sources	T/σ	$B = T\sqrt{\pi a}/K_I$	$K_I/(\sigma/\sqrt{\pi a})$
CCT or MT ($a/W = 0.3$, $H/W = 1.0$)	SGBEM (present)	−1.1554	−1.0286	1.1232
	Chen et al. [15]	−1.1554	−1.0286	1.1232
	Fett [60]	−1.1557	−1.0279	–
	Leevers and Radon [10]	–	−1.0255	–
	Cardew et al. [11]	–	−1.026	–
SENT ($a/W = 0.3$, $H/W = 12$)	SGBEM (present)	−0.6105	−0.3679	1.6597
	Kim and Paulino [36]	−0.6139	−0.3700	1.6594
	Chen et al. [15]	−0.6103	−0.3677	1.6598
	Fett [60]	−0.6141	−0.3664	–
	Sham [13]	−0.6142	−0.3707	1.6570
SENT ($a/W = 0.5$, $H/W = 12$)	SGBEM (present)	−0.4184	−0.1481	2.8241
	Kim and Paulino [36]	−0.4309	−0.1481	2.8237
	Chen et al. [15]	−0.4217	−0.1493	2.8246
	Fett [60]	−0.4182	−0.1481	–
	Sham [13]	−0.4314	−0.1529	2.8210
SENB ($a/W = 0.3$, $H/W = 12$)	SGBEM (present)	−0.0800	−0.0712	1.1235
	Chen et al. [15]	−0.0792	−0.0704	1.1241
	Fett [60]	−0.0771	−0.0671	–
	Sham [13]	−0.0824	−0.0734	1.1220
SENB ($a/W = 0.5$, $H/W = 12$)	SGBEM (present)	0.3986	0.2662	1.4973
	Chen et al. [15]	0.3975	0.2655	1.4972
	Fett [60]	0.3921	0.2620	–
	Sham [13]	0.3911	0.2616	1.4951
DENT ($a/W = 0.3$, $H/W = 12$)	SGBEM (present)	−0.5326	−0.4780	1.1143
	Kim and Paulino [36]	−0.5384	−0.4444	1.2115
	Fett [60]	−0.5319	−0.4720	–
DENT ($a/W = 0.5$, $H/W = 12$)	SGBEM (present)	−0.5521	−0.4725	1.1685
	Kim and Paulino [36]	−0.5597	−0.4454	1.2567
	Fett [60]	−0.5216	−0.4396	–

can be implemented in the present code and used to predict crack initiation angle (see, for example, Ref. [35]).

A potential extension of this SGBEM work includes development of the two-state integral post-processing approach to 3D crack problems. Another possible extension involves fracture mechanics of non-homogeneous materials, such as FGMs, which can make use of the new Green's functions developed by Chan et al. [62] in 2D and

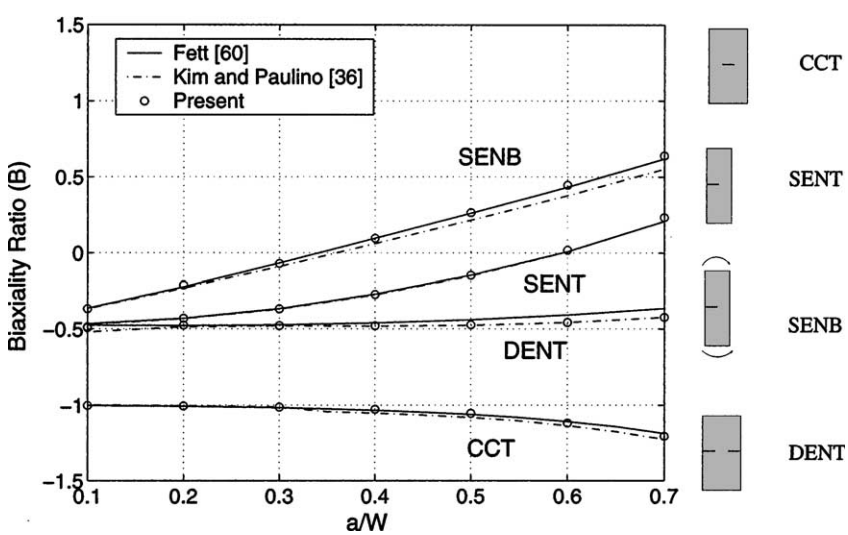

Fig. 13. Biaxiality ratio versus a/W for various fracture specimens.

Martin et al. [63] in 3D. Such Green's function approach allow the boundary element solution of fracture problems in FGMs using a boundary-only approach (i.e. no domain discretization).

Acknowledgements

We acknowledge the support from the Computational Science and Engineering (CSE) Program (Prof. Michael Heath, Director) at the University of Illinois at Urbana-Champaign (UIUC) for the CSE Fellowship award to A. Sutradhar. We thank Dr L.J. Gray, Oak Ridge National Laboratory and Prof. Anh-Vu Phan, South Alabama University, for helping us with the 2D SGBEM elasticity code. We also thank Dr J.-H. Kim for providing the SIF results for the slanted edge crack problem obtained by the M-integral method using the FEM and also for useful suggestions. G.H. Paulino acknowledges the support from the National Science Foundation under grant CMS-0115954 (Mechanics and Materials Program).

Appendix A. Auxiliary fields for SIFs

The angular functions $f_{ij}(\theta)$ in Eqs. (2) and (24) are given by

$$\begin{aligned}
f_{11}^{\mathrm{I}}(\theta) &= \cos\frac{\theta}{2}\left(1-\sin\frac{\theta}{2}\sin\frac{3\theta}{2}\right),\\
f_{11}^{\mathrm{II}}(\theta) &= -\sin\frac{\theta}{2}\left(2+\cos\frac{\theta}{2}\cos\frac{3\theta}{2}\right),\\
f_{22}^{\mathrm{I}}(\theta) &= \cos\frac{\theta}{2}\left(1+\sin\frac{\theta}{2}\sin\frac{3\theta}{2}\right),\\
f_{22}^{\mathrm{II}}(\theta) &= \sin\frac{\theta}{2}\cos\frac{\theta}{2}\cos\frac{3\theta}{2},\\
f_{12}^{\mathrm{I}}(\theta) &= \sin\frac{\theta}{2}\cos\frac{\theta}{2}\cos\frac{3\theta}{2},\\
f_{12}^{\mathrm{II}}(\theta) &= \cos\frac{\theta}{2}\left(1-\sin\frac{\theta}{2}\sin\frac{3\theta}{2}\right)
\end{aligned} \tag{A1}$$

and $g_i(\theta)$ in Eq. (25) is given by

$$\begin{aligned}
g_1^{\mathrm{I}}(\theta) &= \frac{1}{4}\left[(2\kappa-1)\cos\frac{\theta}{2}-\cos\frac{3\theta}{2}\right],\\
g_1^{\mathrm{II}}(\theta) &= \frac{1}{4}\left[(2\kappa+3)\sin\frac{\theta}{2}+\sin\frac{3\theta}{2}\right],\\
g_2^{\mathrm{I}}(\theta) &= \frac{1}{4}\left[(2\kappa+1)\sin\frac{\theta}{2}-\sin\frac{3\theta}{2}\right],\\
g_2^{\mathrm{II}}(\theta) &= -\frac{1}{4}\left[(2\kappa-3)\cos\frac{\theta}{2}+\cos\frac{3\theta}{2}\right].
\end{aligned} \tag{A2}$$

Appendix B. Displacement derivatives of auxiliary fields for determining the T-stress

$$\begin{aligned}
u_{1,1}^{\mathrm{aux}} &= \frac{-f\cos\theta}{\pi E' r}\left(1-\frac{\sin^2\theta}{1-\nu}\right)\\
u_{2,1}^{\mathrm{aux}} &= \frac{+f\sin\theta}{\pi E' r}\left(1-\frac{\cos^2\theta}{1-\nu}\right)\\
u_{1,2}^{\mathrm{aux}} &= \frac{-f\sin\theta}{\pi E' r}\left(1+\frac{\cos^2\theta}{1-\nu}\right)\\
u_{2,2}^{\mathrm{aux}} &= \frac{-f\cos\theta}{\pi E' r}\left(1-\frac{\cos^2\theta}{1-\nu}\right)
\end{aligned} \tag{B1}$$

where E' is given by Eq. (23).

Appendix C. Displacement derivatives of auxiliary fields for SIFs

$$\begin{aligned}
u_{1,1}^{\mathrm{aux}} &= \frac{1}{8\mu\sqrt{2\pi r}}\left[K_{\mathrm{I}}^{\mathrm{aux}}\left((2\kappa-3)\cos\frac{\theta}{2}+\cos\frac{5\theta}{2}\right)\right.\\
&\quad\left.-K_{\mathrm{II}}^{\mathrm{aux}}\left((2\kappa+1)\sin\frac{\theta}{2}+\sin\frac{5\theta}{2}\right)\right]\\
u_{2,1}^{\mathrm{aux}} &= \frac{1}{8\mu\sqrt{2\pi r}}\left[K_{\mathrm{I}}^{\mathrm{aux}}\left(-(2\kappa+3)\sin\frac{\theta}{2}+\sin\frac{5\theta}{2}\right)\right.\\
&\quad\left.-K_{\mathrm{II}}^{\mathrm{aux}}\left((2\kappa-1)\cos\frac{\theta}{2}-\cos\frac{5\theta}{2}\right)\right]\\
u_{1,2}^{\mathrm{aux}} &= \frac{1}{8\mu\sqrt{2\pi r}}\left[K_{\mathrm{I}}^{\mathrm{aux}}\left((2\kappa+1)\sin\frac{\theta}{2}+\sin\frac{5\theta}{2}\right)\right.\\
&\quad\left.+K_{\mathrm{II}}^{\mathrm{aux}}\left((2\kappa+5)\cos\frac{\theta}{2}+\cos\frac{5\theta}{2}\right)\right]\\
u_{2,2}^{\mathrm{aux}} &= \frac{1}{8\mu\sqrt{2\pi r}}\left[K_{\mathrm{I}}^{\mathrm{aux}}\left((2\kappa-1)\cos\frac{\theta}{2}-\cos\frac{5\theta}{2}\right)\right.\\
&\quad\left.+K_{\mathrm{II}}^{\mathrm{aux}}\left(-(2\kappa-5)\sin\frac{\theta}{2}+\sin\frac{5\theta}{2}\right)\right]
\end{aligned} \tag{C1}$$

Appendix D. Integration of the singular terms in M-integral for calculating the T-stress

The contribution of the singular terms in the M-integral for calculating the T-stress is evaluated. Let

$$M = \int_{\Gamma}\{(\sigma_{ik}\varepsilon_{ik}^{\mathrm{aux}}n_1 - (\sigma_{ij}u_{i,1}^{\mathrm{aux}} + \sigma_{ij}^{\mathrm{aux}}u_{i,1})n_j\}\mathrm{d}\Gamma. \tag{D1}$$

By selecting a circular integration path, the coefficients of the singular terms $O(r^{-1/2})$ from the integration over θ from $-\pi$ to $+\pi$ in Eq. (D1) are evaluated. After integration, the first, second and the third term of Eq. (D1) yield

$$\int_{-\pi}^{\pi}\sigma_{ik}\varepsilon_{ik}^{\mathrm{aux}}n_1\,\mathrm{d}\theta = -\frac{1}{210}\frac{f\sqrt{2}K_{\mathrm{I}}(49\kappa-27)}{\pi\sqrt{r\pi}\mu}, \tag{D2}$$

$$-\int_{-\pi}^{\pi} \sigma_{ij} u_{i,1}^{\text{aux}} n_j \, \mathrm{d}\theta = -\frac{1}{105} \frac{f\sqrt{2}K_{\mathrm{I}}(7\kappa+3)}{\pi\sqrt{r\pi}\mu}, \tag{D3}$$

and

$$-\int_{-\pi}^{\pi} \sigma_{ij}^{\text{aux}} u_{i,1} n_j \, \mathrm{d}\theta = -\frac{1}{10} \frac{f\sqrt{2}K_{\mathrm{I}}(3\kappa-1)}{\pi\sqrt{r\pi}\mu}, \tag{D4}$$

respectively. These three terms add to zero.

References

[1] Rice JR. Path-independent integral and the approximate analysis of strain concentration by notches and cracks. J Appl Mech Trans ASME 1968;35(2):379–86.

[2] Anderson TL. Fracture mechanics: fundamentals and applications. Boca Raton, FL: CRC Press LLC; 1995.

[3] Williams JG, Ewing PD. Fracture under complex stress—the angled crack problem. Int J Fract 1972;8(4):416–41.

[4] Ueda Y, Ikeda K, Yao T, Aoki M. Characteristics of brittle failure under general combined modes including those under bi-axial tensile loads. Eng Fract Mech 1983;18(6):1131–58.

[5] Smith DJ, Ayatollahi MR, Pavier MJ. The role of *T*-stress in brittle fracture for linear elastic materials under mixed-mode loading. Fatigue Fract Eng Mater Struct 2001;24(2):137–50.

[6] Cotterell B, Rice JR. Slightly curved or kinked cracks. Int J Fract 1980;16(2):155–69.

[7] Du Z-Z, Hancock JW. The effect of non-singular stresses on crack-tip constraint. J Mech Phys Solids 1991;39(3):555–67.

[8] O'Dowd NP, Shih CF, Dodds JrRH. The role of geometry and crack growth on constraint and implications for ductile/brittle fracture. In: Constraint effects in fracture theory and applications. volume 2 of ASTM STP 1244, American Society for Testing and Materials; 1995. p. 134–59.

[9] Larsson SG, Carlson AJ. Influence of non-singular stress terms and specimen geometry on small-scale yielding at crack tips in elastic–plastic materials. J Mech Phys Solids 1973;21(4):263–77.

[10] Leevers PS, Radon JCD. Inherent stress biaxiality in various fracture specimen. Int J Fract 1982;19(4):311–25.

[11] Cardew GE, Goldthorpe MR, Howard IC, Kfouri AP. On the elastic T-term. Fundamentals of deformation and fracture: Eshelby memorial symposium. 1985.

[12] Kfouri AP. Some evaluations of the elastic T-term using Eshelby's method. Int J Fract 1986;30(4):301–15.

[13] Sham TL. The determination of the elastic T-term using higher-order weight functions. Int J Fract 1991;48(2):81–102.

[14] Wang Y-Y, Parks DM. Evaluation of the elastic *T*-stress in surface-cracked plates using the line-spring method. Int J Fract 1992;56(1):25–40.

[15] Chen CS, Krause R, Pettit RG, Banks-Sills L, Ingraffea AR. Numerical assessment of *T*-stress computation using a *p*-version finite element method. Int J Fract 2001;107(2):177–99.

[16] Sladek J, Sladek V, Fedelinski P. Contour integrals for mixed-mode crack analysis: effect of nonsingular terms. Theor Appl Fract Mech 1997;27(2):115–27.

[17] Nakamura T, Parks DM. Determination of *T*-stress along three-dimensional crack fronts using an interaction integral method. Int J Solids Struct 1992;29(13):1597–611.

[18] Liu GR. Mesh free methods: moving beyond the finite element method. Boca Raton, FL: CRC Press LLC; 2003.

[19] Bonnet M, Maier G, Polizzotto C. Symmetric Galerkin boundary element method. Appl Mech Rev 1998;51(11):669–704.

[20] Bonnet M. Exploiting partial or complete geometrical symmetry in 3D symmetric Galerkin indirect BEM formulations. Int J Numer Meth Eng 2003;57(8):1053–83.

[21] Gray LJ, Griffith B. A faster Galerkin boundary integral algorithm. Commun Numer Meth Eng 1998;14(12):1109–17.

[22] Sirtori S. General stress analysis method by means of integral equations and boundary elements. Meccanica 1979;14:210–8.

[23] Hartmann F, Katz C, Protopsaltis B. Boundary elements and symmetry. Ingenieur Archiv 1985;55(6):440–9.

[24] Sirtori S, Maier G, Novati G, Miccoli S. A Galerkin symmetric boundary element method in elasticity: formulation and implementation. Int J Numer Meth Eng 1992;35(2):255–82.

[25] Gray LJ, Paulino GH. Symmetric Galerkin boundary integral fracture analysis for plane orthotropic elasticity. Comput Mech 1997;20(1–2):26–33.

[26] Gray LJ, Phan A-V, Paulino GH, Kaplan T. Improved quarter-point crack tip element. Eng Fract Mech 2003;70(2):269–83.

[27] Chen FHK, Shield RT. Conservation laws in elasticity of the J-integral type. J Appl Math Phys (ZAMP) 1977;28:1–22.

[28] Yau JF, Wang SS, Corten HT. A mixed-mode crack analysis of isotropic solids using conservation laws of elasticity. J Appl Mech Trans ASME 1980;47(2):335–41.

[29] Wang SS, Corten HT, Yau JF. Mixed-mode crack analysis of rectilinear anisotropic solids using conservation laws of elasticity. Int J Fract 1980;16(3):247–59.

[30] Gosz M, Moran B. An interaction energy integral method for computation of mixed-mode stress intensity factors along non-planar crack fronts in three dimensions. Eng Fract Mech 2002;69(3):299–319.

[31] Dolbow J, Gosz M. On the computation of mixed-mode stress intensity factors in functionally graded materials. Int J Solids Struct 2002;39(9):2557–74.

[32] Rao BN, Rahman S. Mesh-free analysis of cracks in isotropic functionally graded materials. Eng Fract Mech 2003;70(1):1–27.

[33] Kim J-H, Paulino GH. An accurate scheme for mixed-mode fracture analysis of functionally graded materials using the interaction integral and micromechanics models. Int J Numer Meth Eng 2003;58(10):1457–97.

[34] Kim J-H, Paulino GH. The interaction integral for fracture of orthotropic functionally graded materials: evaluation of stress intensity factors. Int J Solids Struct 2003;40(15):3967–4001.

[35] Kim J-H, Paulino GH. *T*-stress, mixed-mode stress intensity factors, and crack initiation angles in functionally graded materials: a unified approach using the interaction integral method. Comput Meth Appl Mech Eng 2003;192(11):1463–94.

[36] Paulino GH, Kim J-H. A new approach to compute *T*-stress in functionally graded materials by means of the interaction integral method. Eng Fract Mech 2004;71(13–14):1907–50.

[37] Kim J-H, Paulino GH. *T*-stress in orthrotropic functionally graded materials: Lekhnitskii and Stroh formalisms. Int J Fract 2004; [in press].

[38] Banerjee PK. The boundary element methods in engineering. London: McGraw-Hill; 1994.

[39] Aliabadi MH. Evaluation of mixed mode stress intensity factors using the path independent integral. In: Proceedings of 12th International Conference on Boundary Element Methods, Southampton. Computational Mechanics Publications; 1990. p. 281–92.

[40] Sladek J, Sladek V. Evaluation of *T*-stresses and stress intensity factors in stationary thermoelasticity by the conservation integral method. Int J Fract 1997;86(3):199–219.

[41] Denda M. Mixed mode I, II and III analysis of multiple cracks in plane anisotropic solids by the BEM: a dislocation and point force approach. Eng Anal Bound Elem 2001;25(4–5):267–78.

[42] Wen PH, Aliabadi MH. A contour integral for the evaluation of stress intensity factors. Appl Math Model 1995;19(8):450–5.

[43] Aliabadi MH. Boundary element formulations in fracture mechanics. Appl Mech Rev 1997;50(2):83–96.

[44] Aliabadi MH. The boundary element method: vol 2. Application in solids and structures. England: Wiley; 2002.

[45] Williams ML. On the stress distribution at the base of a stationary crack. J Appl Mech Trans ASME 1957;24(1):109–14.
[46] Michell JH. Elementary distributions of plane stress. Proc Lond Math Soc 1900;32:35–61.
[47] Timoshenko SP, Goodier JN. Theory of elasticity, 3rd ed. New York: McGraw-Hill; 1987.
[48] Hills DA, Kelly PA, Dai CN, Korsunsky AM. Solution of crack problems: the distributed dislocation technique. The Netherlands: Kluwer Academic Publishers; 1996.
[49] Rizzo FJ. An integral equation approach to boundary value problems of classical elastostatics. Q Appl Math 1967;25:83–95.
[50] Crouch SL. Solution of plane elasticity problems by the displacement discontinuity method. Int J Numer Meth Eng 1976;10:301–43.
[51] Crouch SL, Starfield AM. Boundary element methods in solid mechanics. London: George Allen and Unwin; 1983.
[52] Phan A-V, Napier JAL, Gray LJ, Kaplan T. Symmetric-Galerkin BEM simulation of fracture with frictional contact. Int J Numer Meth Eng 2003;57(6):835–51.
[53] Hölzer SM. The symmetric Galerkin BEM for plane elasticity: scope and applications. In: Hirsch C, editor. Numerical methods in engineering '92. Amsterdam: Elsevier; 1992.
[54] Li S, Mear ME, Xiao L. Symmetric weak form integral equation method for three-dimensional fracture analysis. Comput Meth Appl Mech Eng 1998;151(3–4):435–59.
[55] Henshell RD, Shaw KG. Crack tip finite elements are unnecessary. Int J Numer Meth Eng 1975;9:495–507.
[56] Barsoum RS. On the use of isoparametric finite elements in linear fracture mechanics. Int J Numer Meth Eng 1976;10:25–37.
[57] Gray LJ, Paulino GH. Crack tip interpolation, revisited. SIAM J Appl Math 1998;58(2):428–55.
[58] Kim J-H, Paulino GH. Finite element evaluation of mixed-mode stress intensity factors in functionally graded materials. Int J Numer Meth Eng 2002;53(8):1903–35.
[59] Shbeeb NI, Binienda WK, Kreider KL. Analysis of the driving forces for multiple cracks in an infinite nonhomogeneous plate. Part II. Numerical solutions. J Appl Mech Trans ASME 1999;66(2): 501–6.
[60] Fett T. *T*-stresses in rectangular plates and circular disks. Eng Fract Mech 1998;60(5–6):631–52.
[61] ABAQUS/standard user's manual. Version 6.3, vol. I. Pawtucket, RI, USA: Hibbitt, Karlsson and Sorensen Inc.; 2003.
[62] Chan Y-S, Gray LJ, Kaplan T, Paulino GH. Green's function for a two-dimensional exponentially-graded elastic medium. Proceedings of the Royal Society of London Series A: Mathematical, Physical and Engineering Sciences. 2004. [in press].
[63] Martin PA, Richardson JD, Gray LJ, Berger J. On Green's function for a three-dimensional exponentially-graded elastic solid. Proc R Soc Lond Ser A: Math Phys Eng Sci 2002;458(2024):1931–47.